

ORIGINAL RESEARCH ARTICLE

Altered entropy in the precuneus and posterior cingulate cortex in Alzheimer's disease: A resting functional magnetic resonance imaging study

Aura C. Puche^{1*}, John Fredy Ochoa-Gómez¹, Yésika Alexandra Agudelo-Londoño¹, Jan Karlo Rodas-Marín², Carlos Andrés Tobón-Quintero²

^{1*} Universidad de Antioquia, Antioquia, Colombia. E-mail: aura.puche@udea.edu.co

² Institución Prestadora de Servicios de Salud IPS, Universitaria, Medellín, Colombia.

ABSTRACT

The human brain has been described as a complex system. Its study by means of neurophysiological signals has revealed the presence of linear and nonlinear interactions. In this context, entropy metrics have been used to uncover brain behavior in the presence and absence of neurological disturbances. Entropy mapping is of great interest for the study of progressive neurodegenerative diseases such as Alzheimer's disease. The aim of this study was to characterize the dynamics of brain oscillations in such disease by means of entropy and amplitude of low frequency oscillations from Bold signals of the default network and the executive control network in Alzheimer's patients and healthy individuals, using a database extracted from the Open Access Imaging Studies series. The results revealed higher discriminative power of entropy by permutations compared to low-frequency fluctuation amplitude and fractional amplitude of low-frequency fluctuations. Increased entropy by permutations was obtained in regions of the default network and the executive control network in patients. The posterior cingulate cortex and the precuneus showed differential characteristics when assessing entropy by permutations in both groups. There were no findings when correlating metrics with clinical scales. The results demonstrated that entropy by permutations allows characterizing brain function in Alzheimer's patients, and also reveals information about nonlinear interactions complementary to the characteristics obtained by calculating the amplitude of low frequency oscillations.

Keywords: Functional MRI; Alzheimer's Disease; Permutation Entropy; Default Network; Executive Control Network; Medical Image Processing

ARTICLE INFO

Received: 30 March 2022
Accepted: 7 May 2022
Available online: 12 May 2022

COPYRIGHT

Copyright © 2022 by author(s).
Imaging and Radiation Research is published by EnPress Publisher LLC. This work is licensed under the Creative Commons Attribution-NonCommercial 4.0 International License (CC BY-NC 4.0).
<https://creativecommons.org/licenses/by-nc/4.0/>

1. Introduction

Alzheimer's disease (AD) is the most common cause of dementia^[1]. According to projections made in 2014^[2], the number of people with AD in Colombia by 2020 is 260,000 with an approximate cost of 1 billion pesos^[3]. AD is characterized by an excessive accumulation of extracellular β -amyloid plaques and the presence of intracellular hyperphosphorylated tau protein neurofibrillary tangles, resulting in an atypical configuration that extends throughout the cerebral cortex^[4]. AD has been described by three stages: the preclinical stage, in which atypical accumulation of β -amyloid begins without clinical manifestations; mild cognitive impairment (MCI), which can be amnesic and non-amnesic; and, finally, the dementia stage, in which memory impairment and lack of independence of the individual to perform tasks of daily living are identified. This last stage, in turn, has three phases: mild, moderate and severe^[5].

Different imaging modalities have been widely used for the study of AD. In particular, functional magnetic resonance imaging is considered a technology that could have clinical relevance due to its promising potential for the identification of brain alterations caused by the disease^[6]. The study of brain oscillations by resting functional magnetic resonance imaging (rs-fMRI) through blood-oxygenation-level-dependent (BOLD) signal analysis has demonstrated alterations in the default network (DN) and the executive control network (ECN) in AD patients^[7-10].

The use of connectivity metrics based on graph theory and independent component analysis has allowed the identification of accelerated deterioration in AD subjects in specific brain regions, such as the areas involved in the default network, while in subjects with normal aging, disruptions have been identified with non-uniform occurrence throughout the brain^[11]. On the other hand, the use of spectral metrics such as Amplitude of Low Frequency Fluctuations (ALFF) and its fractional version (fALFF)^[12] have improved the performance of machine learning algorithms for the discrimination of MCI and AD subjects from cognitively normal individuals^[13].

Although rs-fMRI has yielded information related to brain dynamics, it is still not a technique usually used in clinical settings due to factors such as the presence of artifacts in the signals and the absence of *gold standard* metrics for the estimation of brain function^[6,14]. Therefore, some efforts have focused on making methodological innovations that allow understanding brain function from the analysis of interactions of a nonlinear nature that characterize neurophysiological signals^[15]. The use of methods based on information theory allows capturing nonlinear interactions that can be beneficial for the understanding of brain function^[15], and recent studies highlight that the use of nonlinear approaches for the study of brain function provides relevant information for the study in healthy and pathological brains^[16].

Several approaches have been used to estimate brain complexity by nonlinear metrics, among them a variety of approaches for entropy computation^[17]. A less commonly used approach is entro-

py by permutations, a simple, fast and robust method for the analysis of chaotic time series^[18]. This metric has previously been used for BOLD signal analysis in Alzheimer's Disease Neuroimaging Initiative (ADNI) subjects with MCI, AD and controls where a decrease in entropy was found in AD patients compared to subjects with MCI and controls. The study reported significant findings of correlation between the metric and the Mini Mental clinical scales and clinical assessment of dementia. The analysis was performed with BOLD signals of 130 time points and an embedded dimension of 4. The parameters used are highlighted by the authors as a limitation of the study^[19]. To the authors' knowledge, this is the only study performed in AD using the permutation entropy metric, evidencing that to date there are few studies that have used complexity metrics for the analysis of fMRI data in AD^[20].

This study used rs-fMRI data with 164 time points from the OASIS-3 open access initiative (Open Access Series of Imaging Studies: Longitudinal MRI Data in Non-demented and Demented Older Adults^[21] from subjects labeled as cognitively normal (CN and with AD). Brain function was quantified by permutation entropy and compared with ALFF and fALFF for the default network and the executive control network; additionally, the metrics were correlated with clinical scales. The above, with the aim of evaluating whether the use of entropy by permutations provides additional information to that obtained with spectral metrics, on the dynamics of brain oscillations and provides differential characteristics in patients with AD and healthy subjects when evaluated in the brain networks at rest that are mostly affected in AD.

2. Methodology

2.1 Subjects

Structural MRI and functional MRI data labeled as AD and CN were downloaded from the OASIS-3 database^[21], a longitudinal project where several individuals underwent more than one acquisition. Two experts analyzed the clinical information available on the platform of subjects labeled as AD and CN^[21], taking into account information

such as: age, personal history, age of symptom onset, clinical picture recorded over time, evolution of cognitive alterations, scores on neuropsychological tests and available functionality scales. From the review we excluded subjects labeled as AD who during longitudinal follow-up had a subsequent diagnosis of CN, mild clinical picture suggesting an uncertain dementia syndrome, evolution of symptoms that appeared to be dementia due to another condition or neurodegenerative disease, presenting depressive symptoms that could explain the cognitive complaints, having the MRI prior to the onset of symptoms or having a history of a major neurological disease other than AD that could alter the results (such as a history of cerebrovascular disease or encephalocranial trauma).

After performing the clinical review, data from 117 subjects were preprocessed, of which 23 were discarded for excess motion (AD: 12, CN:11) and 1 subject from the CN group was discarded for having outliers in several regions of the default network. Finally, data from 93 subjects (AD: 36, CN:57) were included for further analyses. Although the database does not specifically provide information on disease severity, it was determined by the sum of boxes of the Clinical Dementia Rating Scale Sum of Boxes (CDR-SB) and the Mini-Mental State Examination (MMSE). Since individuals in the AD group are characterized by a $4.5 < \text{CDR-SB} < 9$ they belong to the mild Alzheimer’s category^[22]. Detailed demographic information can be seen in **Table 1**.

Table 1. Demographic information of study subjects

Parameter	AD Mean \pm Standard deviation	CN Mean \pm Standard deviation	Value
n	36	57	-
Sex (female: male)	16:20	24:33	0.48
Age	74.70 \pm 5.89	70.97 \pm 6.52	<0.01
Schooling (years)	15.33 \pm 2.77	15.6S \pm 2.70	0.72
MMSE	25.19 \pm 3.14	28.91 \pm 1.24	<0.01
CDR-SB	3.33 \pm 1.45	0.00 \pm 0.00	<0.01

Source: own elaboration.

2.2 Image acquisition

The rs-fMRI images were acquired with a SIEMENS 3T scanner (MAGNETOM Trio Tim, Siemens, Erlangen, Germany). 164 volumes of 36 slices each and voxel size $4 \times 4 \times 4$ mm were acquired with the parameters: echo time (TE) = 27 ms, repetition time (TR) = 2,200 ms, flip angle (FA) = 90°, matrix size = 64. Additional information related to the acquisition of the images can be found in the OASIS^[23].

2.3 Image processing

Image preprocessing was performed in the CONN toolbox^[24]. A visual inspection was made to discard low quality images. Subsequently, data realignment was performed taking the first slice as reference, temporal correction and registration with the corresponding T1 image. The motion correction report was then inspected; subjects with head motion $>2^\circ$ in rotation and >2 mm in translation in any direction were excluded. Images of all 117 subjects were preprocessed, of which 23 subjects (AD:12,

CN:11) were discarded for excess motion.

The images of the remaining 94 subjects were normalized to the standard space defined by the Montreal Neurological Institute (MNI), preserving the $2 \times 2 \times 2$ mm voxel size. Removal of motion trends, white matter related signals and cerebrospinal fluid was performed. A band-pass filter was applied in the frequency range of 0.01 Hz to 0.1 Hz.

2.4 BOLD signal extraction

The extraction of the signals was performed from the templates proposed by Whitfield-Gabrieli *et al.*^[25] for the default network and the executive control network (**Figure 1**). Masks of each region with number of voxels greater than 50 were used, therefore, 17 BOLD signals were extracted for the default network and 11 BOLD signals were extracted for the executive control network. The process of obtaining the signals was performed with the DPARSFA tool^[26] (DPABI_V4.1_190725). Details of the names of each region involved are given in **Table 2**.

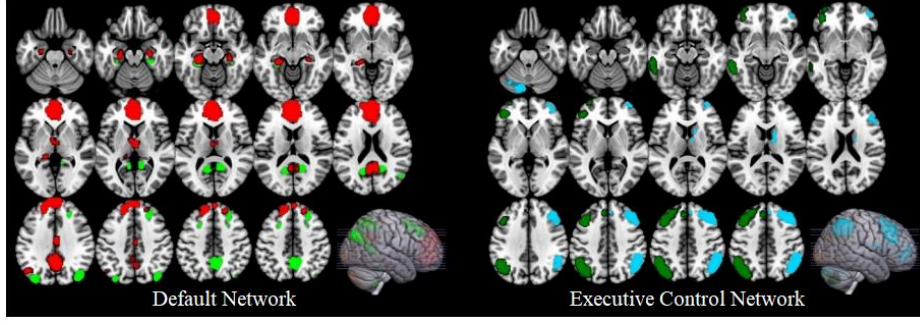


Figure 1. Regions of interest of the default network and the executive control network.

Source: own elaboration.

Table 2. Name of the regions that make up the networks according to the reference template

Label	Default network	Label	Executive Control Network
1	Medial Prefrontal Cortex, Anterior Cingulate Cortex and Frontal Orbitofrontal Cortex (B)	1	Middle Frontal Rotation, Upper Frontal Rotation (I)
2	Angular Rotation (I)	2	Frontal Inferior Rotation, Frontal Orbital Rotation (I)
3	Upper Front Pivot (D)	3	Superior Parietal Lobe, Inferior Parietal Lobe, Precuneus, Angular Gyrus (I)
4	Posterior Cingulate Cortex, Precuneus (B)	4	Giro Temporal Inferior, Giro Temporal Medio (I)
5	Dorsal Anterior Cingulate Cortex (B)	5	Crus I (D)
6	Thalamus (B)	6	Middle Frontal Rotation, Upper Frontal Rotation (D)
7	Hippocampus (I)	7	Medium Front Swing (P)
8	Hippocampus (D)	8	Inferior Parietal Lobe, Supramarginal Gyrus, Angular Gyrus (D)
9	Cortesa. RetrosPEnial, Posterior Cingulate Cortex (I).	9	Upper Front Pivot (D)
10	Middle Frontal Rotation (I)	10	Crus I, Crus II, Lobe VI (D)
11	Parahippocampal Gyrus (I)	11	Caudate nucleus (D)
12	Middle Occipital Twist (I)	-	-
13	Retrospeial Cortex, Posterior Cingulate Cortex (D)	-	-
14	Precuneus (B)	-	-
15	Upper Front Twist, Middle Front Twist (D)	-	-
16	Parahypocampal Gyrus (D)	-	-
17	Angular Rotation. Middle Occipital Twist (D)	-	-

Source: own elaboration. * D: regions located in the right hemisphere; I: regions located in the left hemisphere and B: regions located in both hemispheres.

2.5 BOLD signal analysis

For each DN and ECN region, the spectral measures ALFF and fALFF and the nonlinear metric Permutation Entropy (PE) were applied. All metrics were calculated on signals in the frequency band from 0.01 Hz to 0.1 Hz.

2.5.1 Amplitude of Low Sequence Fluctuations

ALFF is defined as the sum of amplitudes in a frequency band, while fALFF is defined as the fraction of the sum of amplitudes in a frequency band. For a time series of length N defined in (1), the computation of the ALFF and fALFF metrics is represented by (2) and (3), respectively^[27].

$$x(t) = \sum_{k=1}^N [a_k \cos(2\pi f_k t) + b_k \sin(2\pi f_k t)] \quad (1)$$

$$ALFF = \sum_{k: f_k \in [0.01, 0.08]} \sqrt{\frac{a_k^2(f_k) + b_k^2(f_k)}{N}} \quad (2)$$

$$fALFF = \frac{\sum_{k: f_k \in [0.01, 0.08]} \sqrt{\frac{a_k^2(f_k) + b_k^2(f_k)}{N}}}{\sum_{k=1}^N \sqrt{\frac{a_k^2(f_k) + b_k^2(f_k)}{N}}} \quad (3)$$

2.5.2 Entropy by permutations

Permutation entropy is an approach proposed by Bandt *et al.*^[18] for the analysis of complex and chaotic time series, which has the advantage of giving significant results in the presence of observational and dynamic noise, moreover, it is a simple, fast computational and robust method. For a time series $\{\#\} = 1, \dots, \dots, \#$ permutations of order $\#$, the PE is defined by (4), where $\#(\#)$ is defined by (5), where the symbol $\#$ refers to “number”^[18].

$$H(n) = - \sum p(\pi) \log(p(\pi)) \quad (4)$$

$$p(\pi) = \frac{\#\{t \mid t \leq T - n, (x_{t+1}, \dots, x_{t+n}) \text{ has type } \pi\}}{T - n + 1} \quad (5)$$

An embedded delay (#) of (2) and an embedded dimension (#) of (4)^[28], where # and # fulfilled the condition defined by (6) to avoid undersampling of the signals, were used for the PD calculation.

$$m! \leq N - (m - 1) \quad (6)$$

$N = 164$, corresponds to the length of the time series. The parameter # does not have much influence on the entropy of the time series, its value was taken based on the literature reported by electroencephalography studies^[28]. The measurement was standardized by the natural algorithm of #!, where PE reaches its maximum value, (7):

$$PE = \frac{H(n)}{\ln(m!)} \quad (7)$$

2.5.3 Statistical analysis

The effect of age was removed from the metrics by means of linear regression. A two-sample nonparametric statistical test, described by Glerean *et al.*^[29], was used for the comparison between groups, with significance level $p < 0.05$, and correction was performed by means of the False Discovery Rate (FDR, p_fdr) method. Uncorrected p-values (p_unc) were analyzed for multiple comparisons because this was an exploratory study on the PE metric and because it was a study with different sample sizes between groups (CN:57, AD:36). Effect size was calculated with Hedges' g , using the Be Measures of Effect Size Toolbox^[30], the findings are mainly discussed with this measure. Additionally, a correlation analysis was performed using Spearman's correlation index between the clinical rating scales MMSE, CDR-SB and the metrics obtained in the BOLD signal analysis of the AD group.

The metrics were set to a range of 0 to 1 to

improve the visualization of the results by means of box plots.

3. Results

3.1 Default network

A statistically significant increase in entropy was observed in the AD group compared to the CN group in region 10 involving the retrosplenial cortex and posterior cingulate cortex of the left hemisphere, with median effect size value -0.57. The increase in entropy could also be observed in region 4 involving the posterior cingulate cortex and pre-cuneus, with median effect size value -0.57 (**Table 3** and **Figure 2**).

No differences between groups were observed for the ALFF and fALFF metrics, the box plot can be visualized in **Figures S1** and **S2** in the appendix. The values obtained by correlating the metrics with the CDR-SB and MMSE clinical scales for the default network regions can be found in **Tables S1** and **S2**, respectively in the appendix.

3.2 Executive control network

An increase in ALFF was observed in the right caudate nucleus in the AD group, with a median effect size value of -0.43. On the other hand, an increase in entropy was obtained in the AD group compared to the CN group in the following regions: Right Crus I with effect size -0.38, right middle frontal gyrus with effect size -0.35, right caudate nucleus with effect size -0.37 and in the region involving Crus I, Crus II and right lobule VI with effect size -0.38. The previously described differences presented statistical significance without FDR correction (**Table 4**, **Figure 3** and **Figure 4**).

No between-group differences were observed for the fALFF metric. The box plot can be seen in **Figure S3** in the appendix.

The values obtained by correlating the metrics with the CDR-SB and MMSE clinical scales for the executive control network regions can be found in **Tables S1** and **S2**, respectively, in the appendix.

Table 3. *P*-values and effect size for the 17 default network regions

ROI	ALFF			fALFF			PE		
	p1_unc	p2_unc	ES	p1_unc	p2_unc	ES	p1_unc	p2_unc	ES
1	0.40	0.60	-0.01	0.43	0.57	0.05	0.21	0.79	0.15
2	0.29	0.71	0.08	0.09	0.91	0.16	0.08	0.92	0.35
3	0.47	0.53	-0.03	0.72	0.28	-0.08	0.54	0.46	0.01
4	0.47	0.53	-0.04	0.46	0.54	-0.07	0.99	0.01	-0.57
5	0.53	0.47	-0.05	0.77	0.23	-0.16	0.47	53	0.06
6	0.88	0.12	-0.29	0.70	0.30	-0.10	0.24	0.76	0.08
7	0.85	0.15	-0.32	0.45	0.55	0.03	0.08	0.92	0.37
8	0.50	0.50	-0.12	0.27	0.73	0.12	0.18	0.82	0.29
9	0.45	0.55	-0.02	0.51	0.49	-0.01	10.0	0.00*	-0.57
10	0.40	0.60	-0.03	0.65	0.35	-0.12	0.59	0.41	-0.04
11	0.86	0.14	-0.28	0.77	0.23	-0.09	0.84	0.16	-0.19
12	0.26	0.74	0.09	0.36	0.64	0.07	0.16	0.84	0.26
13	0.59	0.41	-0.13	0.52	0.48	-0.04	0.81	0.19	-0.07
14	0.29	0.71	0.09	0.80	0.20	-0.25	0.87	0.13	-0.28
15	0.44	0.56	-0.07	0.53	0.47	0.00	0.87	0.13	-0.23
16	0.82	0.18	-0.25	0.83	0.17	-0.19	0.58	0.42	0.00
17	0.37	0.63	0.02	0.59	0.41	-0.12	0.55	0.45	0.06

Source: own elaboration. p1_unc: uncorrected *p*-value for CN tail > AD; p2_unc: uncorrected *p*-value for queue CN < AD; ES: effect size; I: left; D: right; *: region with p_fdr < 0.05 (p1_fdr:1.0, p2_fdr:0.04).

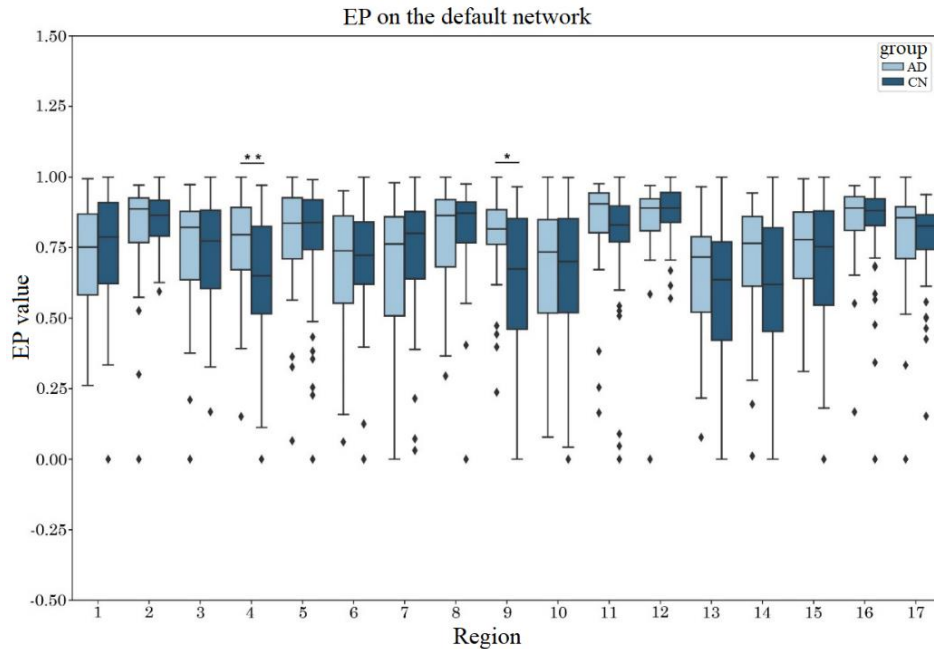


Figure 2. PD in the default network, statistically significant difference $*p \leq 0.05$ in the region involving the left retrosplenial cortex and posterior cingulate cortex, **: uncorrected in the region involving the posterior cingulate cortex and precuneus.

Source: own elaboration.

Table 4. *P*-values and effect sizes for the 11 regions of the executive control network

ROI	ALFF			fALFF			PE		
	p1_unc	p2_unc	EN	p1_unc	p2_unc	EN	p1_unc	p2_unc	EN
1	0.47	0.53	0.01	0.88	0.12	-0.24	0.34	0.66	0.09
2	0.21	0.79	0.17	0.41	0.59	0.05	0.56	0.44	-0.04
3	0.41	0.59	0.06	0.20	0.80	0.18	0.24	0.76	0.16
4	0.85	0.15	-0.23	0.82	0.18	-0.20	0.78	0.22	-0.17
5	0.71	0.29	-0.12	0.58	0.42	-0.04	0.97	0.03	-0.38
6	0.41	0.59	0.05	0.83	0.17	-0.21	0.29	0.71	0.12
7	0.12	0.88	0.25	0.08	0.92	0.31	0.95	0.05	-0.35
8	0.52	0.48	-0.01	0.40	0.60	0.06	0.17	0.83	0.22
9	0.39	0.61	0.06	0.14	0.86	0.25	0.73	0.27	-0.13
10	0.41	0.59	0.05	0.79	0.21	-0.17	0.96	0.04	-0.38
11	0.98	0.02	-0.43	0.13	0.87	0.25	0.96	0.04	-0.37

Source: own elaboration. p1_unc: uncorrected *p*-value for CN tail > AD; p2_unc: uncorrected *p*-value for CN tail < AD; ES: effect size; I: left; D: right.

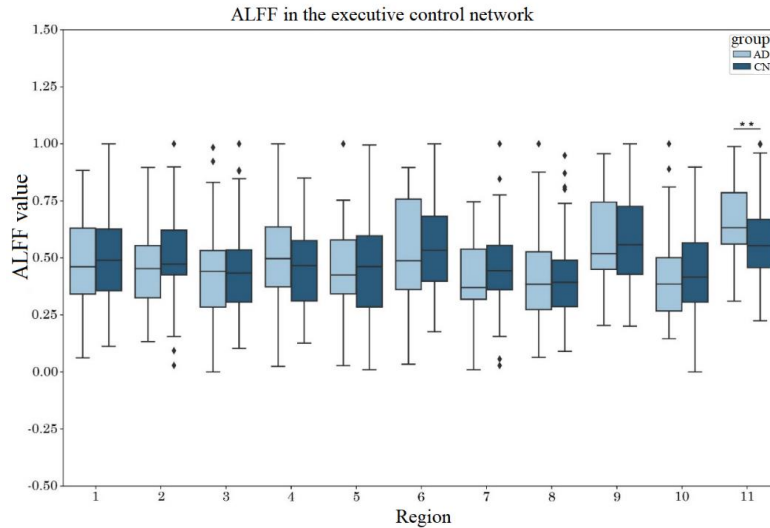


Figure 3. ALFF: statistically significant differences were found in the executive control network. **: without correction in the right caudate nucleus. Source: own elaboration.

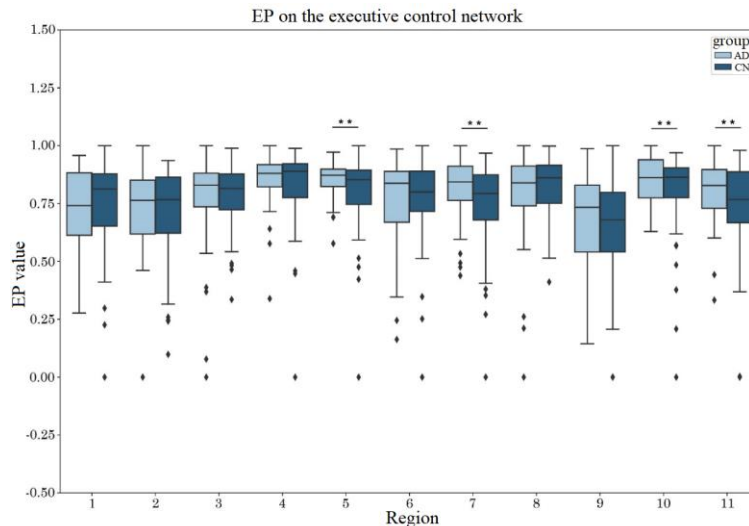


Figure 4. EP: in the executive control network, statistically significant differences. **: no correction in the right Crus I region, right middle frontal gyrus, the region involving the right Crus I, Crus II and lobe VI, and in the right caudate nucleus. Source: own elaboration.

4. Discussion

In this study we investigated the potential of the permutation entropy metric to extract information about brain complexity in regions that make up the default network and the executive control network, its performance was compared with the spectral metrics ALFF and fALFF in AD patients and healthy subjects. An increase in EP was found in AD patients in both networks, additionally an increase in ALFF was found in AD patients in the executive control network.

When analyzing the default network in patients, an increase in PD was found in the region involving

the posterior cingulate cortex and the precuneus. On the other hand, the study on the executive control network revealed an increase of ALFF in the caudate nucleus and an increase of PD in the right hemisphere regions: middle frontal gyrus, caudate nucleus and the region comprising Crus I, Crus II and lobule VI. In line with these findings, it has been reported that disorganization in the functional connectivity of this region is of importance for the development of dementia in AD^[31]. The posterior cingulate cortex is considered a key region of the default network in which changes in brain connectivity have been reported in AD^[32], with high discriminatory power between it and control subjects^[33]. From a pathological point of view, the

precuneus and posterior cingulate cortex have been associated with the full development of AD, where tau protein retention and astrogliosis have been reported, in addition to significant alterations in functional connectivity^[31]. A structural MRI study reported that the posterior cingulate cortex is one of the most vulnerable regions involved in AD pathophysiology. Accelerated impairment of multiple cognitive domains was identified in individuals with a higher rate of gray matter volume atrophy of this region^[34]. In a meta-analysis of connectivity with rs-fMRI has been reported in AD subjects with no connectivity between the default network and the limbic system, given mainly by the precuneus and posterior cingulate areas^[8]. Another study evaluating intranetwork connectivity by default showed increased connectivity between the posterior cingulate with the parahippocampal cortex and the precuneus in people with AD compared to controls^[35]. However, it should be noted that the findings of resting connectivity in AD are contradictory. Apparently, connectivity in the default network may be modified according to the stage of dementia, and there may be a decrease in posterior parietal and temporal areas at symptom onset and an increase in anterior frontal areas with disease progression; whether this is due to possible compensation or a change due to the pathophysiology of abnormal protein deposition itself has not been clarified^[36].

Contrary to the results of this investigation, previous rs-fMRI studies^[19,37,38] have reported reduced complexity in AD compared to healthy subjects. One such study^[19] found decreased EP in the AD group when compared to the control group in temporal, occipital and frontal lobe regions (right hemisphere: inferior temporal gyrus, wedge, middle occipital gyrus and superior occipital gyrus; left hemisphere: middle frontal gyrus, superior frontal gyrus, anterior cingulate gyrus and wedge. On the other hand, the same study reported increased PD in the early-stage mild cognitive impairment group when compared to the control group in the right hemisphere regions: inferior temporal gyrus, middle frontal gyrus, wedge, middle occipital gyrus and superior occipital gyrus. It is important to highlight that the referenced study did not start from the

study of regions that are part of the brain networks at rest that are mostly affected in Alzheimer's disease; instead, the analysis was performed on 8 regions belonging to 5 clusters that showed significant differences after obtaining the EP metric over all brain voxels. The study data were taken from the ADNI initiative. On the other hand, the study by Zheng *et al.*^[37] used the multiscale entropy metric to quantify the complexity of BOLD signals in subjects with early mild cognitive impairment, late mild cognitive impairment and control subjects taken from the ADNI initiative. The study reported decreased complexity in the left fusiform gyrus region and rostral anterior cingulate cortex in the early mild cognitive impairment group. The methodological approach consisted of generating multiscale entropy maps for each subject over all brain voxels. With respect to the study by Grieder *et al.*^[38], they used the multiscale entropy metric to quantify the complexity of BOLD signals in subjects with mild cognitive impairment and control subjects recruited at the Memory Clinic of the Department of Geriatrics, Karolinska University Hospital, Huddinge, Sweden. The analysis was performed on regions of the default network defined by Shirer *et al.*^[25], of which reported decreased entropy at the global level and at the nodal level reported reduction in the right hippocampus. Results are reported without correction for multiple comparisons. As common limitations of the previously cited studies it is highlighted that the ADNI initiative did not publicly provide information on AD-related risk factors^[19] and it is noted that previous studies have suggested that the ADNI diagnostic criterion of mild cognitive impairment has a high false-positive rate^[37].

The study by Boccardi *et al.*^[39] evaluated the impact of aging on dementia from a cellular approach, in which late-onset AD can be seen as a manifestation of reduced energy production, resulting in increased entropy. The authors suggest that the accumulation of age-related modifications, as well as the depletion of mitochondria, could be responsible for the poor ability of the brain to adapt its brain structures and functions. On the other hand, the relationship between entropy during healthy aging and AD has been recently explored by rs-fMRI and brain entropy mapping (BEN) met-

rics^[40] in groups of control individuals (n = 54, age: 65–95 years), memory-impaired controls (n = 27, age 65–95 years), early mild cognitive impairment (n = 58, age: 56–89 years), late mild cognitive impairment (n = 38, 57–88 years) and subjects with AD (n = 34, 56–87 years). The referenced study reported the following behavior of BEN in the four groups of interest. The comparison is described with respect to the control group: slight increase in control individuals with memory compromise, more noticeable increase in the early mild cognitive impairment group. For the late mild cognitive impairment stage, a slight decrease was reported that later became a more noticeable reduction in the AD group, the reduction in BEN in the late stages of dementia is related by the author to a failed compensation phenomenon^[40]. According to Tagliazucchi *et al.*^[41] and the literature^[42], the marked reduction in BEN present in the late stages of dementia results in accelerated deterioration of brain functions that require high entropy levels to be functionally flexible. The findings of this study, described as Alzheimer’s type dementia in section 2.1, are in line with the behavior described by the early-onset mild cognitive impairment group in the study by Wang^[40], highlights this aspect for being the only study describing the behavior of entropy in 5 cognitive stages of interest in the study of AD. However, through reference^[38], contradictions are evident in the findings of studies performed from rs-fMRI data in AD with the aim of quantifying the complexity of BOLD signals in AD, suggesting that additional studies are needed in the field, which also include longitudinal follow-up and provide additional information on subject selection criteria.

ALFF is a metric that allows the identification of spontaneous neural activity of specific brain regions through the intensity of the BOLD signal. It has been used as a characteristic metric to improve the performance of machine learning algorithms for discriminating MCI and AD subjects from cognitively normal individuals^[13]. The ALFF and entropy metrics are theoretically unrelated, however, in this study an increase in ALFF and PE was found in the caudate nucleus. The study by Song *et al.*^[43] conducted with a cohort of healthy subjects reported positive correlations of medium to high magni-

tude between BEN and fALFF in the orbitofrontal cortex and posterior inferior temporal cortex. On the other hand, it reported high magnitude negative correlations between BEN and fALFF in visual cortex, anterior inferior temporal cortex, motor network, precuneus, and lateral parietal cortex, suggesting that fALFF and BEN are mutually independent. The previously referenced study suggests that BEN may provide more complete information on brain function, especially in regions where there are no associations between BEN and fALFF, in line with the findings of our study.

Among the limitations of this research is the use of unpaired groups by sex and age. It is important to note that OASIS-3 is a database that includes subjects ranging in age from 42 years to 95 years who were recruited over the course of 30 years. Some of the subjects included in this study were initially labeled as cognitively normal who developed AD dementia over time and others entered the OASIS-3 initiative with a diagnosis of dementia of Alzheimer’s type, for both cases the review performed by clinical experts allowed excluding subjects with AD label who could have symptoms explained by other clinical conditions or not have a clear diagnosis, based on the information provided by the clinical history available in the database. It should be noted that the database does not specify the clinical stage of dementia in which the subjects are found, so it had to be determined from scale measurements that, while reliable, do not match the clinical criteria. The analysis approaches reported by previous studies limit the comparability of the findings of this study, mainly because of the uncertainty about the stage of subjects classified as AD or ADNI mild and late cognitive impairment, in addition to the use of metrics other than PD to quantify the complexity of BOLD signals. In addition, some limitations were found related to the presence of artifacts in the images and changes in diagnosis during longitudinal follow-up that decreased the initial sample. Although the size of the signals is of longer duration compared to the EP study performed by Wang *et al.*^[19], performing this analysis on signals with more than 164 volumes would be beneficial to assess the entropy in the AD continuum due to the 24 states defined by the em-

bedded dimension equal to 4.

While statistical tests give considerable inference of the relationship between two or more variables, allowing interpretability within the data, their predictive accuracy is not their main strength, so future research should consider the potential effects of machine learning to complement the results presented, where one would have the ability to generate a model from the nonlinear PE metric and obtain reproducible predictions, with a more robust analysis in the search for discriminant patterns between groups, in this case AD vs CN, which would also allow obtaining greater predictive power with the addition of more samples from the different populations and reducing the presence of artifacts^[44]. Consequently, according to certain studies^[16,45], the use of functional connectivity metrics of nonlinear dynamic fluctuations as baseline data for analysis has been suggested, since it provides a better pathophysiological characterization of neural networks in populations with neurodegenerative diseases, in addition to being data that can be efficiently manipulated by artificial neural networks, since they allow the modeling of nonlinear relationships in fields of great complexity.

5. Conclusions

The current study identified increased entropy in regions of the default network and the executive control network in AD patients. The differential finding of greatest magnitude was manifested in the posterior cingulate cortex and the precuneus. The implemented methodology allowed us to demonstrate the ability of the permutation entropy metric to capture information about brain function in Alzheimer's disease compared to spectral metrics. The metric should be explored in longitudinal studies and in longer duration signals to evaluate its potential to capture functional patterns related to AD.

Acknowledgments

This work was supported by the Administrative Department of Science, Technology and Innovation (Colciencias), for the project "Identification of Preclinical Biomarkers in Alzheimer's Disease through Longitudinal Monitoring of Brain Electri-

cal Activity in Populations with Genetic Risk", code 111577757635.

Data were provided by OASIS-3: Principal Investigators: Benzinger T, Marcus D, Morris J; NIH P50 AG00561, P30 NS09857781, P01 AG026276, P01 AG003991, R01 AG043434, UL1 TR000448, R01 EB009352.

Part of the financing of the authors was provided by the strengthening of medical and health sciences programs with young talent and regional impact of the Ministry of Science, Technology and Innovation (MinCiencias)–RC 752–2018. These resources were managed by the Academic Corporation for the Study of Tropical Pathologies of the University of Antioquia.

Conflicts of interest

The authors declare that they have no conflict of interest.

References

1. World Health Organization. The global dementia observatory reference guide world health organization [Internet]. Geneva, Switzerland; 2018. Available from: <https://apps.who.int/iris/bitstream/handle/10665/272669/WHO-MSD-MER-18.1-eng.pdf>
2. Takeuchi Y, Ariza-Araujo Y, Prada S. P3-349: Prevalence estimates of dementia in Colombia (2005–2020): Transitions and stage of disease. *Alzheimer's & Dementia* 2014; 10(4S): 758. doi: 10.1016/j.jalz.2014.05.1442.
3. Prada SI, Takeuchi Y, Ariza Y. Costo monetario del tratamiento de la enfermedad de Alzheimer en Colombia (Spanish) [Monetary cost of treatment of Alzheimer's disease in Colombia]. *Acta Neurológica Colombiana* 2014; 30(4).
4. Busche MA, Hyman BT. Synergy between amyloid- β and tau in Alzheimer's disease. *Nature Neuroscience* 2020; 23(10): 1183–1193.
5. Vermunt L, Sikkes SAM, van den Houtet A, *et al.* Duration of preclinical, prodromal, and dementia stages of Alzheimer's disease in relation to age, sex, and APOE genotype. *Alzheimer's & Dementia* 2019; 15(7): 888–898. doi: 10.1016/j.jalz.2019.04.001
6. Dickerson BC, Agosta F, Filippi M. fMRI in Neurodegenerative diseases: From scientific insights to clinical applications. In: *fMRI techniques and protocols*. New York: Humana Press; 2016. p. 699–739. doi: 10.1007/978-1-4939-5611-1_23.
7. Agosta F, Pievani M, Geroldi C, *et al.* Resting state fMRI in Alzheimer's disease: Beyond the default mode network. *Neurobiology of Aging* 2012; 33(8): 1564–1578. doi: 10.1016/j.neurobiolaging.2011.06.007.

8. Badhwar AP, Tam A, Dansereau C, *et al.* Resting-state network dysfunction in Alzheimer's disease: A systematic review and meta-analysis. *Alzheimer's & Dementia: Diagnosis, Assessment & Disease Monitoring* 2017; 8(1): 73–85. doi: 10.1016/j.dadm.2017.03.007
9. Weiler M, Aya F, Lilian FPM, *et al.* Default mode, executive function, and language functional connectivity networks are compromised in mild Alzheimer's disease. *Current Alzheimer Research* 2014; 11(3): 274–282. doi: 10.2174/1567205011666140131114716.
10. Zhao Q, Lu H, Metmer H, *et al.* Evaluating functional connectivity of executive control network and frontoparietal network in Alzheimer's disease. *Brain Research* 2018; 1678: 262–272. doi: 10.1016/j.brainres.2017.10.025
11. Dennis EL, Thompson PM. Functional brain connectivity using fMRI in aging and Alzheimer's disease. *Neuropsychology Review* 2014; 24(1): 49–62. doi: 10.1007/s11065-014-9249-6
12. Lv H, Wang Z, Tong E, *et al.* Resting-state functional MRI: Everything at Nonexperts have always wanted to know. *American Journal of Neuroradiology* 2018; 39(8): 1390–1399. doi: 10.3174/ajnr.A5527
13. Yang L, Yan Y, Wang Y, *et al.* Gradual disturbances of the amplitude of low-frequency fluctuations (ALFF) and fractional ALFF in Alzheimer spectrum. *Frontiers in Neuroscience* 2018; 12: 975. doi: 10.3389/fnins.2018.00975.
14. Poldrack PA. The role of fMRI in Cognitive Neuroscience: Where do we stand? *Current Opinion in Neurobiology* 2008; 18(2): 223–227. doi: 10.1016/j.conb.2008.07.006
15. Timme NM, Lapish C. A tutorial for information theory in neuroscience. *eNeuro* 2018; 5(3). doi: 10.1523/ENEURO.0052-18.2018
16. Moguilner S, Garc á AM, Sanz Perl Y, *et al.* Dynamic brain fluctuations outperform connectivity measures and mirror pathophysiological profiles across dementia subtypes: A multicenter study. *Neuroimage* 2021; 225: 117522. doi: 10.1016/j.neuroimage.2020.117522
17. Yang A, Tsai SJ, Lin C, *et al.* A strategy to reduce bias of entropy estimates in resting-state fMRI signals. *Frontiers in Neuroscience* 2008; 12: 398. doi: 10.3389/fnins.2018.00398
18. Bandt C, Pompe B. Permutation entropy: A natural complexity measure for time series. *Physical Review Letters* 2001; 88(17).
19. Wang B, Niu Y, Miao L, *et al.* Decreased complexity in Alzheimer's disease: Resting-state fMRI evidence of Brain entropy mapping. *Frontiers in Aging Neuroscience* 2017; 9. doi: 10.3389/fnagi.2017.00378.
20. Sun J, Wang B, Niu Y, *et al.* Complexity analysis of EEG, MEG, and fMRI in mild cognitive impairment and Alzheimer's disease: A review. *Entropy* 2020; 22(2). doi: 10.3390/e22020239.
21. LaMontagne PJ, Benzinger TLS, Morris JC, *et al.* OASIS-3: Longitudinal neuroimaging, clinical, and cognitive dataset for normal aging and Alzheimer disease. *MedRxiv* 2019; 2–37. doi: 10.1101/2019.12.13.19014902
22. O'Bryant SE, Waring SC, Cullum CM, *et al.* Staging dementia using clinical dementia rating scale sum of boxes scores: A Texas Alzheimer's research consortium study. *Archives of Neurology* 2008; 65(8): 1091–1095. doi: 10.1001/archneur.65.8.1091.
23. OASIS. OASIS-3: Imaging methods & data dictionary [Intrnet]. 2018. Available from: https://www.oasis-brains.org/files/OASIS-3_Imaging_Data_Dictionary_v1.8.pdf.
24. Whitfield-Gabrieli S, Nieto-Castanon A. Conn: A functional connectivity toolbox for correlated and anticorrelated brain networks. *Brain Connectivity* 2012; 2(3): 125–141. doi: 10.1089/brain.2012.0073.
25. Shirer WR, Ryali S, Rykhlevskaia E, *et al.* Decoding subject-driven cognitive states with whole-brain connectivity patterns. *Cerebral Cortex* 2011; 22(10): 158–165. doi: 10.1093/cercor/bhr099.
26. Yan C, Wang X, Zuo X, *et al.* DPABI: Data processing & analysis for (resting-state) brain imaging. *Neuroinformatics* 2016; 14(3): 339–351. doi: 10.1007/s12021-016-9299-4
27. Zuo X, Di Martino A, Kelly C, *et al.* The oscillating brain: complex and reliable. *Neuroimage* 2010; 49(2): 1432–1445. doi: 10.1016/j.neuroimage.2009.09.037
28. Riedl M, Müller A, Wessel N. Practical considerations of permutation entropy: A tutorial review. *European Physical Journal: Special Topics* 2013; 222(2): 249–262. doi: 10.1140/epjst/e2013-01862-7.
29. Glerean E, Pan RK, Salmi J, *et al.* Reorganization of functionally connected brain subnetworks in high-functioning autism. *Human Brain Mapping* 2015; 37: 1066–1079. doi: 10.1002/hbm.23084.
30. Hentschke H, Stüttgen MC. Computation of measures of effect size for neuroscience data sets. *European Journal of Neuroscience* 2011; 34(12): 1887–1894. doi: 10.1111/j.1460-9568.2011.07902.x.
31. Yokoi T, Watanabe H, Yamaguchi H, *et al.* Involvement of the precuneus/posterior cingulate cortex is significant for the development of Alzheimer's disease: A PET (THK5351, PiB) and resting fMRI study. *Frontiers in Aging Neuroscience* 2018; 10. doi: 10.3389/fnagi.2018.00304.
32. Dillen KNH, Jacobs HIL, Kukulja J, *et al.* Aberrant functional connectivity differentiates rerosplenial cortex from posterior cingulate cortex in prodromal Alzheimer's disease. *Neurobiology of Aging* 2016; 44: 114–126. doi: 10.1016/j.neurobiolaging.2016.04.010.
33. Koch W, Teipel S, Mueller S, *et al.* Diagnostic power of default mode network resting state fMRI in the detection of Alzheimer's disease. *Neurobiology of Aging* 2012; 33(3): 466–478. doi: 10.1016/j.neurobiolaging.2010.04.013.
34. Lee P, Chou K, Chung C, *et al.* Posterior cingulate cortex network predicts Alzheimer's disease progression. *Frontiers in Aging Neuroscience* 2020; 12.

608667. doi: 10.3389/fnagi.2020.608667.
35. Li C, Li Y, Zheng L, *et al.* Abnormal brain network connectivity in a triple-network model of Alzheimer's disease. *Journal of Alzheimer's Disease* 2019; 69(1): 237–252. doi: 10.3233/JAD-181097.
 36. Jagust W. Imaging the evolution and pathophysiology of Alzheimer disease. *Nature Reviews Neuroscience* 2018; 19(11): 687–700. doi: 10.1038/s41583-018-0067-3.
 37. Zheng H, Onoda K, Nagai A, *et al.* Reduced dynamic complexity of BOLD signals differentiates mild cognitive impairment from normal aging. *Frontiers in Aging Neuroscience* 2020; 12: 90. doi: 10.3389/fnagi.2020.00090.
 38. Grieder M, Wang DJJ, Dierks T, *et al.* Default mode network complexity and cognitive decline in mild Alzheimer's disease. *Frontiers in Neuroscience* 2018; 12: 770. doi: 10.3389/fnins.2018.00770.
 39. Boccardi V, Comanducci C, Baroni M, *et al.* Of energy and entropy: The ineluctable impact of aging in old age dementia. *International Journal of Molecular Sciences* 2017; 18(12): 2672. doi: 10.3390/ijms18122672.
 40. Wang Z. Brain entropy mapping in healthy aging and Alzheimer's disease. *Frontiers in Aging Neuroscience* 2020; 12: 372. doi: 10.3389/fnagi.2020.596122
 41. Tagliazucchi E, Balenzuela P, Fraiman D, *et al.* Criticality in large-scale brain fMRI dynamics unveiled by a novel point process analysis. *Frontiers in Physiology* 2012; 3: 15. doi: 10.3389/fphys.2012.00015.
 42. Haimovici A, Tagliazucchi E, Balenzuela P, *et al.* Brain organization into resting state networks emerges at criticality on a model of the human connectome. *Physical Review Letters* 2013; 110(17): 178101. doi: 10.1103/PhysRevLett.110.178101.
 43. Song D, Chang D, Zhang J, *et al.* Associations of brain entropy (BEN) to cerebral blood flow and fractional amplitude of low-frequency fluctuations in the resting brain. *Brain Imaging and Behavior* 2019; 13(5): 1486–1495. doi: 10.1007/s11682-018-9963-4.
 44. Mera-Jiménez L, Ochoa-Gómez JF. Convolutional neural networks for the classification of independent rs-fMRI components. *Tecnológicas* 2021; 24(50): 97–115.
 45. Liégeois R, Li J, Kong R, *et al.* Resting brain dynamics at different timescales capture distinct aspects of human behavior. *Nature Communications* 2019; 10(1): 1–9. doi: 10.1038/s41467-019-10317-7.

Appendix

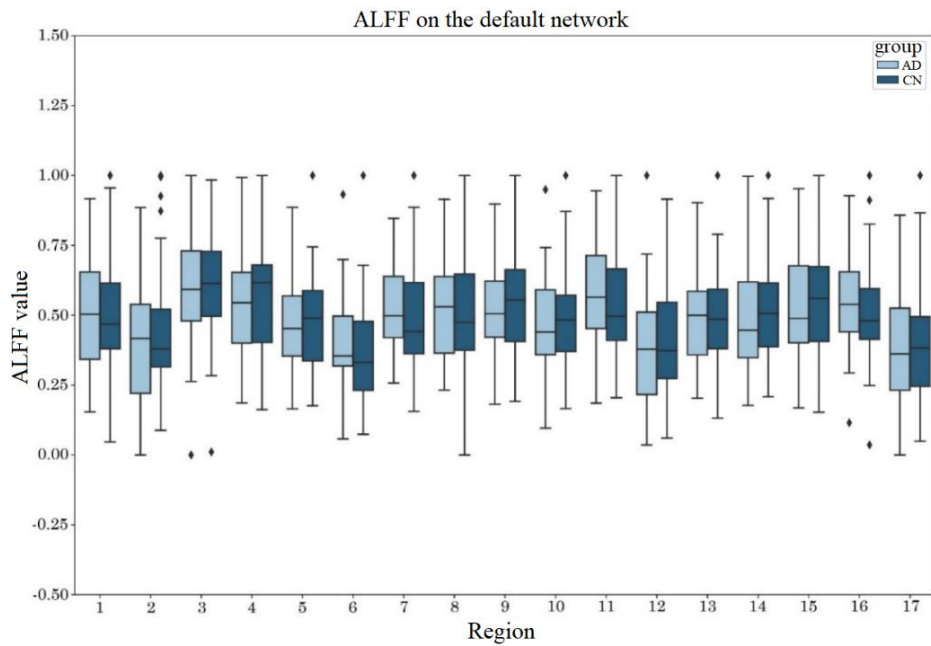


Figure S1. ALFF in the default network, with no statistically significant findings.

Source: own elaboration.

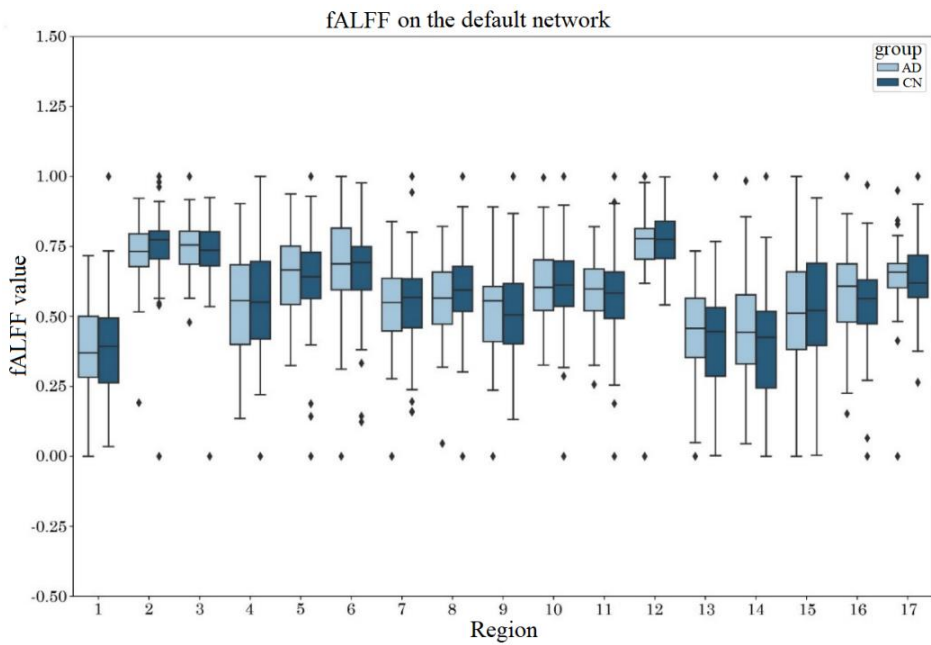


Figure S2. fALFF in the default network, with no statistically significant findings.

Source: own elaboration.

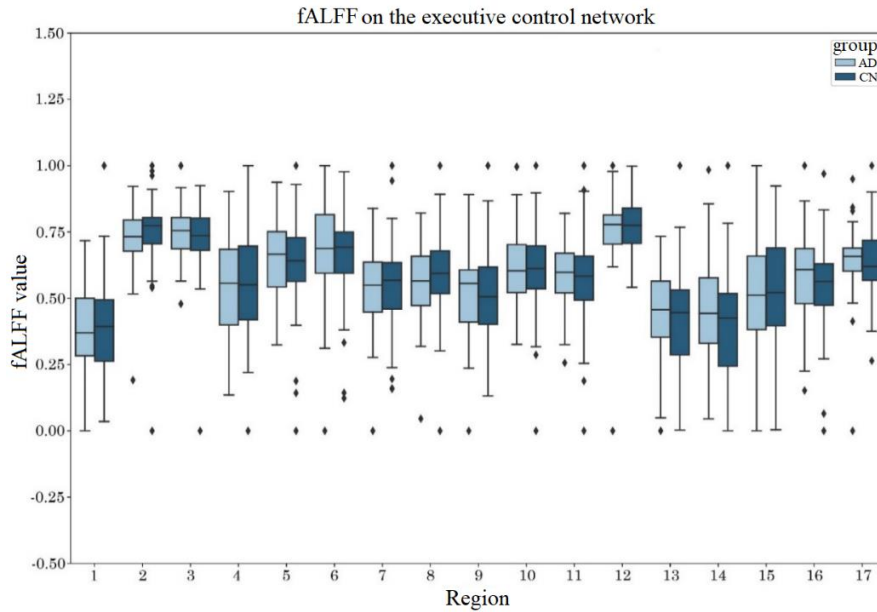


Figure S3. fALFF in the executive control network, with no statistically significant findings.

Source: own elaboration.

Table S1. Correlation of the metrics with the CDR-SB scale for the default network regions

ROI	ALFF		fALFF		PE	
	r	P	r	P	r	P
1	0.01	0.94	-0.13	0.45	-0.14	0.41
2	-0.10	0.55	-0.27	0.11	-0.04	0.83
3	0.07	0.66	-0.12	0.48	0.04	0.82
4	0.06	0.74	0.05	0.79	0.16	0.34
5	0.10	0.58	0.13	0.46	-0.17	0.31
6	0.05	0.76	-0.05	0.79	0.02	0.92
7	0.05	0.77	0.02	0.90	-0.13	0.45
8	0.06	0.72	-0.01	0.96	0.24	0.17
9	0.07	0.70	-0.01	0.95	0.06	0.75
10	0.13	0.44	-0.01	0.94	0.01	0.97
11	0.09	0.59	0.25	0.15	-0.16	0.34
12	-0.06	0.73	0.01	0.94	0.12	0.49
13	0.11	0.54	0.08	0.66	0.03	0.86
14	0.10	0.55	0.03	0.84	0.15	0.38
15	0.04	0.80	0.06	0.71	-0.06	0.73
16	0.05	0.77	-0.03	0.87	-0.20	0.24
17	0.05	0.76	0.27	0.12	0.21	0.21

Source: own elaboration.

Table S2. Correlation of metrics with the MMSE scale for the default network regions

ROI	ALFF		fALFF		PE	
	r	P	r	P	r	P
1	0.11	0.53	0.12	0.48	0.07	0.68
2	0.07	0.68	0.03	0.88	0.12	0.47
3	0.17	0.32	-0.06	0.74	0.07	0.67
4	0.15	0.38	-0.05	0.78	-0.03	0.87
5	0.03	0.85	-0.07	0.68	0.11	0.54
6	0.13	0.44	-0.02	0.90	0.11	0.54
7	-0.14	0.43	0.08	0.66	0.13	0.46
8	-0.08	0.65	-0.12	0.50	-0.31	0.07
9	0.11	0.54	-0.06	0.74	0.07	0.68
10	0.09	0.61	0.11	0.51	0.32	0.06
11	-0.13	0.46	0.05	0.75	0.14	0.41
12	0.05	0.79	0.07	0.68	0.07	0.66
13	0.04	0.82	0.05	0.78	0.09	0.62
14	0.13	0.44	0.02	0.93	0.02	0.92
15	0.12	0.47	-0.05	0.75	0.07	0.67
16	-0.08	0.65	0.05	0.79	0.47	0.00
17	0.02	0.93	0.00	0.98	-0.13	0.44

Source: own elaboration.

Table S3. Correlation of metrics with the CDR-SB scale for executive control network regions

ROI	ALFF		fALFF		PE	
	r	P	R	P	r	P
1	0.16	0.35	-0.16	0.35	-0.18	0.30
2	0.08	0.62	-0.02	0.89	-0.28	0.10
3	0.01	0.98	-0.05	0.79	0.13	0.45
4	0.02	0.92	-0.01	0.95	-0.13	0.46
5	0.16	0.35	0.07	0.68	0.07	0.71
6	0.07	0.69	-0.15	0.38	-0.09	0.60
7	-0.02	0.91	0.03	0.85	0.03	0.84
8	0.03	0.86	0.13	0.44	0.02	0.90
9	0.01	0.93	0.10	0.55	-0.03	0.85
10	0.21	0.22	-0.06	0.73	0.31	0.06
11	0.04	0.83	0.34	0.04	0.16	0.36

Source: own elaboration.

TABLE S4. Correlation of metrics with the MMSE scale for executive control network regions

ROI	ALFF		fALFF		PE	
	r	P	R	P	r	P
1	0.14	0.43	0.07	0.67	0.19	0.27
2	0.04	0.82	0.21	0.22	0.15	0.37
3	0.04	0.83	-0.04	0.83	0.17	0.33
4	-0.18	0.28	-0.05	0.76	-0.04	0.80
5	-0.10	0.54	0.02	0.93	-0.16	0.36
6	0.11	0.52	-0.05	0.76	0.07	0.67
7	0.09	0.62	-0.12	0.49	0.27	0.10
8	0.02	0.91	-0.20	0.24	0.02	0.92
9	0.14	0.42	-0.08	0.65	0.01	0.97
10	-0.05	0.78	0.11	0.51	0.11	0.53
11	0.03	0.84	-0.25	0.14	0.04	0.80

Source: own elaboration